

https://doi.org/10.1070/QEL16470

Photon echo of an ultranarrow optical transition of $^{167}Er^{3+}$ in $^{7}LiYF_4$ crystals

M.M. Minnegaliev, E.I. Baibekov, K.I. Gerasimov, S.A. Moiseev, M.A. Smirnov, R.V. Urmancheev

Abstract. **The longitudinal and transverse relaxation times for a transition between hyperfine sublevels of the lower electronic states of the $^4I_{15/2}$ and $^4I_{9/2}$ multiplets of $^{167}Er^{3+}$ ions in $^7LiYF_4$ crystals have been determined for the first time using two-pulse and stimulated photon echo measurements in zero magnetic field at a temperature of 4 K. The decay of the photon echo signal has been shown to be modulated, which is tentatively attributed to the superhyperfine interaction of the $^{167}Er^{3+}$ ions with their $^{19}F^-$ nearest neighbours. The contributions of various types of interaction to the ultranarrow linewidth (~24 MHz) of the transition in question are discussed. Our results demonstrate that this optical transition of the $^{167}Er^{3+}$ ion in $^7LiYF_4$ crystals is potentially attractive for use in Raman quantum memory schemes.**

Keywords: *photon echo, optical spectroscopy, ultranarrow optical absorption lines, rare-earth ions, Er, $LiYF_4$, Raman quantum memory.*

1. Introduction

The study of the spectroscopic and kinetic properties of rare-earth (RE) ions in crystals is an important issue because low concentrations of RE ions in a crystal provide an effective spectroscopic probe for gaining insight into various types of interaction between atoms and ions in solids and elaborating theoretical concepts in this area of physics [1, 2]. Moreover, RE-doped crystals are widely used as laser materials, quantum-electronic devices [3], scintillators [4], crystalline phosphors, etc. [5]. The long phase relaxation times of optical, Zeeman and hyperfine transitions in RE ions and the small inhomogeneous linewidth of these transitions in crystals make such systems potentially attractive as key components of basic quantum information processing devices. One such device is a quantum memory (QM): a necessary element of a scalable linear optical quantum computer [6, 7] and a quantum repeater, required for making long-haul (over 300 km) quantum communication links [8].

To date, a large number of protocols have been proposed for creating an RE-based QM in crystals [9–12]. Protocols based on photon echo in an off-resonant Raman scheme [13–15] offer a number of advantages, but ultranarrow optical transitions (tens of megahertz or even narrower) are needed to implement them.

It is well known that RE (Er, Nd and Ho) ions in a $LiYF_4$ crystal have ultranarrow optical absorption lines (tens of megahertz) [16–19] and that the use of monoisotopic crystals (or crystals containing isotopically enriched lithium in the case of interest) leads to further narrowing of optical lines, because there is no isotope shift, so that in some instances superhyperfine splitting can be observed directly in optical absorption spectra [20].

Erbium ions in $LiYF_4$ have attracted increased interest [21–23] from the viewpoint of creating a quantum repeater based on a QM in an off-resonant Raman scheme, because they have optical transitions in two transmission windows (around 0.8 and 1.5 μm) of optical fibre. Gerasimov et al. [24] carried out a detailed spectroscopic study of these transitions between hyperfine sublevels, which made it possible to obtain important information about possible three-level schemes for an off-resonant Raman QM. The phase relaxation time of Er^{3+} in $LiYF_4$ was determined by photon echo measurements on the $^4I_{15/2} - {}^4F_{9/2}$ (0.65 μm) [16] and $^4I_{15/2} - {}^4I_{13/2}$ (1.5 μm) [22] transitions at a temperature of ~1.5 K in a magnetic field above 2 T, which allowed relaxation processes in the system of erbium ions to be significantly suppressed. In this study, we observed for the first time photon echo of an ultranarrow (24 MHz) optical transition between hyperfine sublevels of the Er^{3+} $^4I_{15/2}$ and $^4I_{9/2}$ multiplets (0.8 μm) at a higher temperature (4 K), in the absence of an external magnetic field. Below, we present the results of those experiments.

2. Experimental results and discussion

We studied $^7LiYF_4$:$^{167}Er^{3+}$ crystals (0.005 at % Er) grown by S.L. Korableva and her collaborators at Kazan Federal University. Figure 1 shows a schematic of the experimental setup. A sample was placed in a Montana Instruments closed cycle cryostat and cooled to a temperature of 4 K. The light source used in our high-resolution laser spectroscopy experiments and photon echo signal measurements was a Tekhnoscan TIS-SF-777 cw Ti:sapphire laser. This laser system has a built-in stabilisation module based on a thermostatted external Fabry–Perot interferometer, which ensures a rather narrow laser emission linewidth (under 5 kHz) and high temporal stability of the laser frequency (which varied at a rate no faster than 5 kHz s^{-1}).

To measure absorption spectra, the laser frequency was continuously varied over 20 GHz by changing the length of the thermostatted external Fabry–Perot interferometer. The laser frequency sweep nonlinearity was then corrected using

M.M. Minnegaliev, K.I. Gerasimov, S.A. Moiseev, M.A. Smirnov, R.V. Urmancheev Kazan Quantum Center (KAI-KVANT), A.N. Tupolev Kazan National Technical University (KAI), ul. Karla Marksa 10, 420111 Kazan, Tatarstan, Russia;
e-mail: mansur@kazanqc.org, kigerasimov@mail.ru;
E.I. Baibekov Kazan (Volga Region) Federal University, Kremlevskaya ul. 18, 420008 Kazan, Tatarstan, Russia

Received 7 July 2017
Kvantovaya Elektronika **47** (9) 778–782 (2017)
Translated by O.M. Tsarev

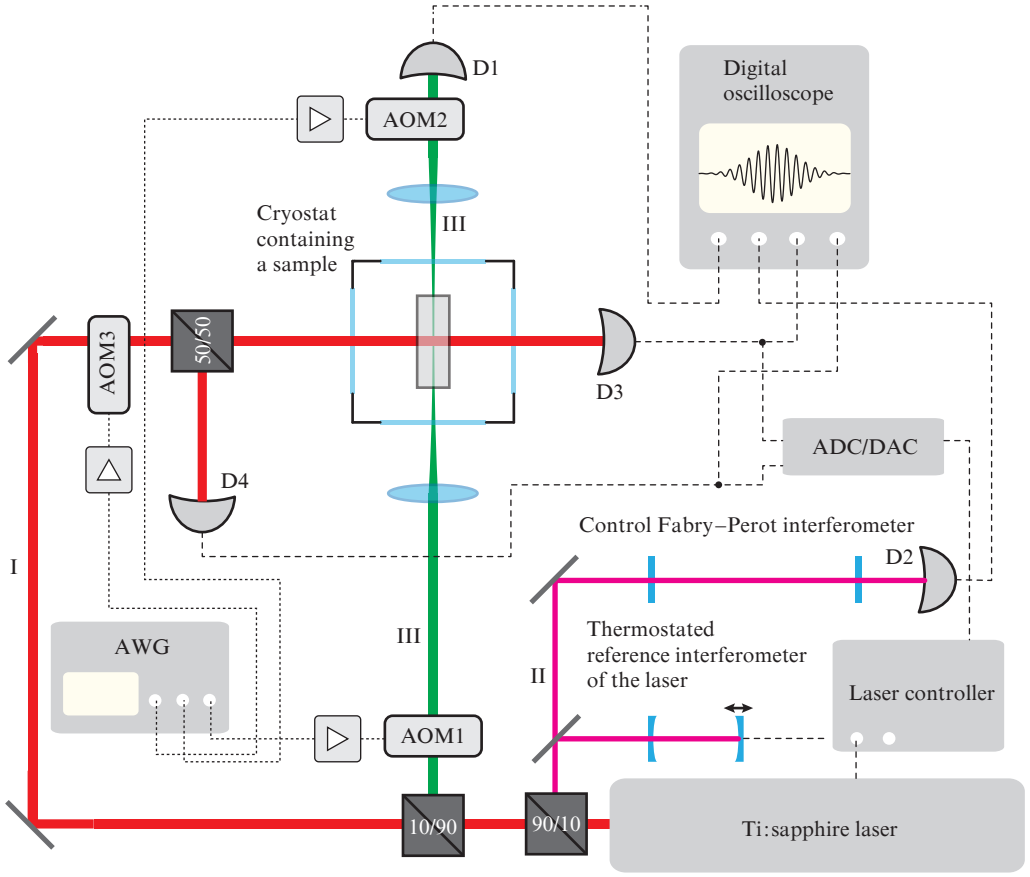

Figure 1. Simplified schematic of the experimental setup used in the high-resolution laser spectroscopy experiments and photon echo signal measurements: (AOM) acousto-optic modulator; (AWG) arbitrary waveform generator; (D) detector; (I) optical channel for measuring absorption spectra; (II) laser frequency stabilisation/control channel; (III) optical channel for photon echo signal measurements.

transmission peaks of a control Fabry–Perot interferometer, which were measured concurrently with the absorption spectrum. The free spectral range of the control Fabry–Perot interferometer was 354.4 MHz. The acousto-optic modulator AOM3 was used in double-pass mode and served to vary the laser frequency in a narrow range (~150 MHz). This ensured more accurate spectral absorption linewidth measurements compared to the spectral measurements with the 20-GHz frequency sweep and subsequent conversion of the laser emission frequency relative to the peaks of the external Fabry–Perot interferometer. Here and in what follows, the AOMs were controlled using a Rigol Model DG5352 arbitrary waveform generator (AWG). Signals from the detectors were recorded by a Tektronix DPO7104C digital oscilloscope.

Owing to an improved $^{7}LiYF_4:Er^{3+}$ crystal growth process, the linewidth of the $^{4}I_{15/2} - {}^{4}I_{9/2}$ hyperfine transitions was reduced by about a factor of 4 compared to that in a previously grown crystal [24]. The inhomogeneous width of the narrowest and strongest absorption line was 24 MHz (Fig. 2). This value approaches the record small (16 MHz) inhomogeneous broadening of the absorption line obtained by Thiel et al. [21] for the $^{4}I_{15/2} - {}^{4}I_{13/2}$ optical transition (1.5 μm) of $^{170}Er^{3+}$ ions in such a crystal. Subsequent photon echo measurements were performed on the transition between the fifth and first hyperfine sublevels of the lower electronic states of the $^{4}I_{15/2}$ and $^{4}I_{9/2}$ multiplets, respectively. The inset in Fig. 2 shows the absorption spectrum of this transition. When this spectrum was taken, the laser frequency was measured using AOM3. As pointed out above, this ensured more accurate measurements of the inhomogeneous linewidth.

In the optical channel for photon echo signal measurements, input light pulses with a required shape and duration were generated using AOM1, and AOM2 protected the sensitive detector D1 (Thorlabs PDA120A/M) from intense input pulses and allowed light to pass only during the echo signal measurement.

Our results indicate that, in photon echo signal measurements on ultranarrow transitions (30 or more acquired echo signals), a major contribution to the signal intensity measurement error is made by the long-term laser frequency drift. In connection with this, we produced and utilised an additional long-term laser frequency stabilisation system. To compensate for the long-term drift of the reference lines of the reference interferometer, we used the absorption signal of the strongest absorption line of the $^{4}I_{15/2} - {}^{4}I_{13/2}$ transition of $^{167}Er^{3+}$ ions in the $^{7}LiYF_4$ crystal [24], i.e. of the line that was used in the photon echo measurements. To this end, we utilised the optical probe channel that was used before to measure absorption spectra (Fig. 1). The probe frequency corresponding to about half the strongest absorption signal was adjusted using AOM3, which operated in this case in single-pass mode. When the laser frequency was changed, the deviation signal from detectors D3 and D4 (Thorlabs DET100A/M), fed through an analogue-to-digital converter (ADC), was analysed in a control computer and then used to correct the length of the reference interferometer and the laser

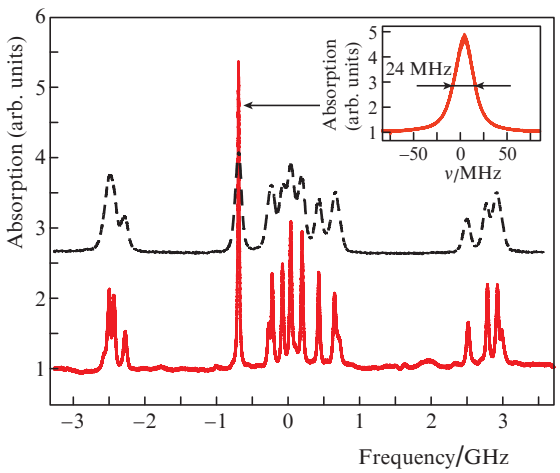

Figure 2. Spectra of the $^{7}LiYF_4:^{167}Er^{3+}$ (0.005 at %) crystals for the $^4I_{15/2}(\Gamma_{56}) - {}^4I_{9/2}(\Gamma_{78})$ transition at $T = 4$ K and $\boldsymbol{E} \| c \perp \boldsymbol{k}$ (where $\boldsymbol{E}$ and $\boldsymbol{k}$ are the electric field vector and wave vector, respectively, and c is the fourfold rotation axis of the crystals). The dashed line represents the spectrum of the crystal studied by Gerasimov et al. [24] and the solid line represents the spectrum of the crystal used in this study. The zero on the frequency axis corresponds to $\nu = 370.574$ THz. The inset shows the strongest absorption line, which was used in subsequent photon echo experiments.

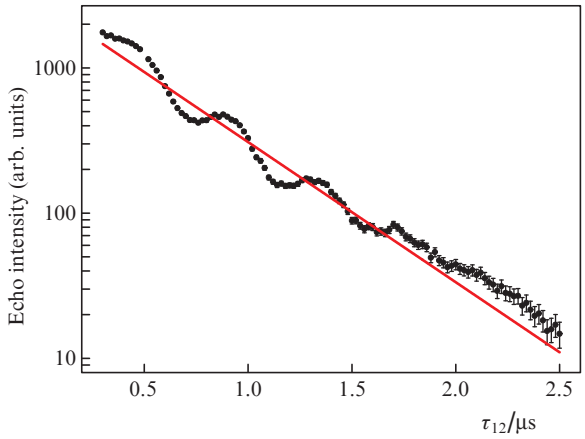

Figure 3. Semilog graph of the two-pulse photon echo signal intensity vs. time delay between the pulses for a $^{7}LiYF_4:^{167}Er^{3+}$ crystal in zero magnetic field at a temperature of 4 K. The photon echo signal was observed for the strongest line of the $^4I_{15/2}(\Gamma_{56}) - {}^4I_{9/2}(\Gamma_{78})$ transition ($\boldsymbol{E} \| c \perp \boldsymbol{k}$) using 100-ns Gaussian pulses. The solid line, obtained by fitting the experimental data, corresponds to a transverse relaxation time of the transition $T_2 = 1.80 \pm 0.07$ μs.

frequency through a digital-to-analog converter (DAC) and laser controller, respectively. Owing to this, the resultant long-term laser frequency drift was reduced from 44 MHz h^{-1} (without the described stabilisation algorithm) to 100 kHz h^{-1} [25]. To further reduce the photon echo intensity measurement error, the mechanical vibrations of the sample due to the operation of the cryogenic station were minimised over the time of a single echo measurement. To this end, the triggering of a pulse train was synchronised with the operation cycle triggering signal of the cryogenic station and the delay (~480 ms) of the triggering of the pulse train relative to this signal was experimentally adjusted so as to minimise echo intensity variations in different measurements. The measurement repetition rate was then determined by the operation cycle frequency of the cryogenic station and was ~0.8 Hz.

The phase relaxation time T_2 for the optical transition under study was determined by two-pulse photon echo measurements. In those experiments, we used 100-ns Gaussian pulses. Figure 3 shows a semilog graph of the measured photon echo signal intensity vs. time delay between the first and second pulses. The vertical bars represent the experimentally estimated error in our photon echo intensity measurements, which is determined by many factors (laser frequency instability, mechanical vibrations of the sample, shot noise and various types of noise in the detector and measuring system) and is thus difficult to assess theoretically. Each data point of the graph in Fig. 3 was obtained by averaging the echo signal intensity I_e over 30 measurements. To estimate error for five different I_e values, measurements were repeated 20 times and the standard deviation was calculated. The error thus evaluated as a function of I_e was then represented as $S = aI_e + b\sqrt{I_e} + c$, where a, b and c are fitting parameters. The S values for each data point in Figs 3 and 4 correspond to the magnitude of the error.

If we neglect amplitude modulation, which has the form of beating (discussed below), the present experimental data can be sufficiently well represented by the exponential relation $I_e(t) = I_0\exp(-4t/T_2)$, with a phase relaxation time $T_2 = 1.80 \pm 0.07$ μs (the solid line in Fig. 3).

It should be noted that we were the first to detect a photon echo signal for this transition at a temperature of 4 K in zero magnetic field. In particular, no photon echo was detected in the crystal studied by Gerasimov et al. [24] under similar conditions. Even when crystals with similar concentrations were cooled to a temperature of ~1.5 K, no photon echo signal was detected previously in the absence of an external magnetic field [22]. To determine the phase relaxation time for the $^4I_{15/2} - {}^4I_{13/2}$ optical transition, Marino et al. [22] carried out experiments in an external magnetic field of ~2.2 T. The observed photon echo signal decay kinetics could be represented by an exponential relation and the phase relaxation time was 1.4 μs if the magnetic field was directed along the c axis of the crystal. If the magnetic field was perpendicular to the symmetry axis of the crystal, the phase relaxation time was 4.7 μs. Thiel et al. [21] measured the phase relaxation time for the same optical transition in a $LiYF_4:Er^{3+}$ (0.005 at %) crystal in an external magnetic field of 5.4 T perpendicular to the c axis of the crystal, which was cooled to a temperature of 1.3 K. Due to spectral diffusion, the photon echo signal decay kinetics could be described by the Mims expression [26] with parameters $T_M = 12$ μs and $x = 2.3$. A photon echo signal was also detected for the $^4I_{15/2} - {}^4F_{9/2}$ transition by Ganem et al. [27] and Macfarlane et al. [28] in a crystal placed in an external magnetic field from 2.9 to 5 T and cooled to a temperature of ~1.5 K. The phase memory time T_M was 4.1 ($x = 1.7$) to 10 μs ($x = 2.4$), depending on the strength of the external magnetic field and its orientation with respect to the axis of the crystal. Thus, we are led to conclude that the improved growth conditions and quality of the $LiYF_4:^{167}Er^{3+}$ crystal used in this study led to not only a considerable decrease in the inhomogeneous absorption linewidth (by a factor of 4) but also an increase in the phase relaxation time, which allowed us to detect a photon echo signal for the $^4I_{15/2} - {}^4I_{9/2}$ transition in this crystal and measure it as a function of time in zero magnetic field at a relatively high temperature (4 K).

Since there is no luminescence from the $^4I_{9/2}$ multiplet, the longitudinal population relaxation time T_1 was determined

using stimulated photon echo measurements with a varied delay between the second and third pulses. In that experiment, we used Gaussian optical pulses of 300-ns duration. Figure 4 shows the measured stimulated photon echo signal intensity as a function of the delay between the two control pulses. Also shown is the magnitude of the error measured as described above. In the case of an ideal two-level system, the corresponding theoretical curve has a simple, exponential form: $I(\tau_{23}) = I_0\exp(-2\tau_{23}/T_1)$. At the same time, the present experimental data are much better represented by the sum of two exponentials: $I(\tau_{23}) = I_0[A_1 \times \exp(-2\tau_{23}/\tilde{T}_{11}) + A_2\exp(-2\tau_{23}/\tilde{T}_{12})]$, with $\tilde{T}_{11} \cong 1.1 \pm 0.25$ μs, $\tilde{T}_{12} \cong 7.5 \pm 0.9$ μs, $A_1 = 0.75$ and $A_2 = 0.25$. The fitting results are shown in Fig. 4 by the solid line. We think that the longitudinal relaxation time can be estimated at $\tilde{T}_{12}$, the time of the same order as T_2 = 1.8 μs. Note that, for $\tau_{23} \leqslant T_2$, the time dependence of the stimulated photon echo intensity may be contributed by the primary echo of the first two pulses, which accounts for the presence of one more contribution, with a relaxation time $\tilde{T}_{11}$, in the $I(\tau_{23})$ data.

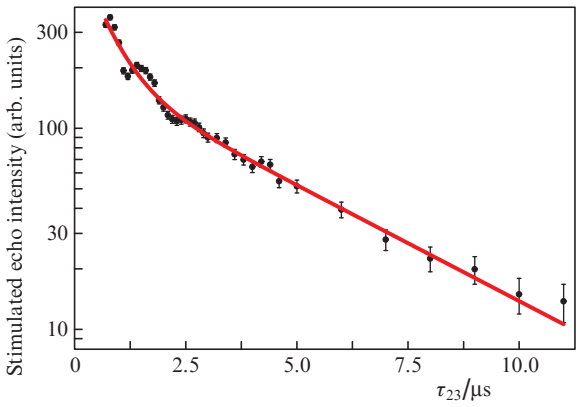

Figure 4. Semilog graph of the stimulated photon echo signal intensity vs. time delay between the second and third pulses for a $^{7}LiYF_4$:$^{167}Er^{3+}$ crystal in zero magnetic field at a temperature of 4 K and Gaussian pulse duration of 300 ns. The solid line represents a fit to the function $I(\tau_{23}) = I_0(A_1\exp(-2\tau_{23}/\tilde{T}_{11}) + A_2\exp(-2\tau_{23}/\tilde{T}_{12}))$ with the following parameters: $\tilde{T}_{11} \cong 1.1 \pm 0.25$ μs, $\tilde{T}_{12} \cong 7.5 \pm 0.9$ μs, $A_1 = 0.75$ and $A_2 = 0.25$.

It is important to note that each of the experimental curves presented in Figs 3 and 4 demonstrates not only an exponential decay but also echo signal intensity beating. The beat frequency was about 2.5 MHz in the case of pulses of 100-ns duration and ~1 MHz at a pulse duration of 300 ns. The Rabi frequency of ideal π-pulses of 300 and 100 ns duration was 1.7 and 5 MHz, respectively. At a pulse duration of 300 ns, the lack of visible oscillations at a frequency of 2.5 MHz can be interpreted as evidence that the observed echo signal modulation is related to the spectral pulse width. In Fig. 3, ~1-MHz beating is not seen because the beat period (~1 μs) is comparable to the transverse relaxation time of the system.

We assume that the observed photon echo signal modulation is due to superhyperfine interactions of the erbium ions with ligands. The nearest neighbours of an RE ion substituting for an Y^{3+} ion on a site with local symmetry S_4 are eight fluorine ions (four on each of the two inequivalent sites), separated from it by $r_1 = 0.223$ nm and $r_2 = 0.226$ nm. The electron paramagnetic resonance spectra of RE-doped $LiYF_4$ crystals are known to often have a resolved superhyperfine structure [29]. The superhyperfine interaction of a rare-earth ion with the nuclear spin of ^{19}F ($I = 1/2$, $\gamma/2\pi = 40.05$ MHz T^{-1}) splits the energy levels of the ion by $h\nu_g$ and $h\nu_e$ (where the subscripts g and e refer to the ground and excited state splitting frequencies of the erbium ion) and entangles the electronic and nuclear states. As a consequence, the photon echo signal exhibits beating at frequencies ν_g and ν_e, as well as at the combination frequencies $\nu_g + \nu_e$ and $|\nu_g - \nu_e|$ [30]. A major contribution to the superhyperfine interaction of RE ions with ligands is made by the magnetic dipole interaction between the erbium 4*f* electrons and the nuclear spin of the ligand and the hyperfine interaction due to electron density transfer from the s- and p-electron shells of the ligands to the RE ion as a consequence of covalency effects.

Let us estimate the former contribution. As a result of the magnetic dipole interaction, the nuclear spin of a ligand at a point with coordinates $\boldsymbol{r}$ relative to the RE ion becomes oriented along the local magnetic field produced by the electrons of the ion. The interaction energy is

$$V_{eN} = \frac{r^2\boldsymbol{M}\boldsymbol{m}_N - 3(\boldsymbol{r}\boldsymbol{M})(\boldsymbol{r}\boldsymbol{m}_N)}{r^5}, \qquad (1)$$

where $\boldsymbol{m}_N = \gamma\hbar\boldsymbol{I}$ is the magnetic moment of the nucleus of the ligand, and the operator of the magnetic moment of the RE ion, $\boldsymbol{M}$, is projected onto the electronic state (ground state $|\psi_g\rangle$ or excited state $|\psi_e\rangle$) so that $\boldsymbol{M} = \mu_B\langle\psi|\boldsymbol{L} + 2\boldsymbol{S}|\psi\rangle$ (where $\boldsymbol{L}$ and $\boldsymbol{S}$ are the total orbital momentum and total spin operators for the 4*f* electron shell). This matrix element was calculated using wave functions obtained previously for the hyperfine sublevels of the $^{167}Er^{3+}$ ion [24]. For the optical transition under investigation, only the projection of the moment $\boldsymbol{M}$ along the *c* axis of the crystal differs from zero: $M_z = \pm g_\parallel\mu_B/2$, where $g_\parallel$ =3.13 and 3.72 are the electron *g*-factors of the $^4I_{15/2}$ and $^4I_{9/2}$ multiplets, respectively. From (1), we find the superhyperfine splitting frequency:

$$\nu = \frac{g_\parallel\mu_B\gamma}{4\pi r^3}\sqrt{1 + 3\cos^2\theta}, \qquad (2)$$

where $\theta_1 = 67.6°$ and $\theta_2 = 38.6°$ are the angles between the *c* axis and the direction to the ligands in positions 1 and 2. Thus,

$$\nu_{1g} = 6.3 \text{ MHz}, \quad \nu_{1e} = 7.5 \text{ MHz},$$
$$\nu_{2g} = 8.5 \text{ MHz}, \quad \nu_{2e} = 10.1 \text{ MHz}. \qquad (3)$$

We can make the following modulation frequency combinations similar to the experimentally observed frequencies: $\nu_{2g} - \nu_{1e} = 1.0$ MHz, $\nu_{1e} - \nu_{1g} = 1.2$ MHz, $\nu_{2g} - \nu_{1g} = 2.2$ MHz and $\nu_{2e} - \nu_{1e} = 2.6$ MHz. No beating was detected at frequencies above 5 MHz because of the limited spectral width of the pulses used.

3. Conclusions

The present results demonstrate that the quality of $LiYF_4$:Er^{3+} crystals has a significant effect on the homogeneous and inhomogeneous linewidths of their optical transitions. One of the crystals grown in this study, $^{7}LiYF_4$:$^{167}Er^{3+}$, has been shown to have a record narrow (~24 MHz) absorption line, which is about a factor of 4 narrower than that in previously

studied crystals [24]. This suggests that such crystals are potentially attractive for use in Raman quantum memory schemes. The reduced homogeneous transition width allowed us to perform the first measurements of the longitudinal and transverse relaxation times for the transition between hyperfine sublevels of the lower electronic states of the $^4I_{15/2}$ and $^4I_{9/2}$ multiplets even in zero external magnetic field at a relatively high temperature (4 K). We have experimentally demonstrated intensity modulation of the primary and stimulated photon echo signals, which we attribute to the superhyperfine interaction of the erbium ions with ligands. The magnetic dipole contribution to the superhyperfine interaction has been estimated and the theoretical calculation results have been compared to experimental data.

Acknowledgements. We are grateful to B.Z. Malkin for useful discussions and for his assistance in interpreting the theoretical results and to S.L. Korableva for performing the crystal growth work. This research was supported by the Russian Science Foundation (Grant No. 14-12-01333P).

References

1. Al'tshuler S.A., Kozyrev B.M. *Electron Paramagnetic Resonance in Compounds of Transition Elements* (New York: Academic, 1974; Moscow: Nauka, 1972).
2. Abragam A., Bleaney B. *Electron Paramagnetic Resonance of Transition Ions* (Oxford: Clarendon, 1970; Moscow: Mir, 1972) Vol. 1.
3. Kaminskii A.A. *Laser Crystals* (New York: Springer, 1981; Moscow: Nauka, 1975).
4. Tsoulfanidis N., Landsberger S. *Measurement and Detection of Radiation* (CRC Press, 2015).
5. Znamenskii N.V., Malyukin Yu.V. *Spektry i dinamika opticheskikh perekhodov redkozemel'nykh ionov v kristallakh* (Spectra and Dynamics of Optical Transitions of Rare-Earth Ions in Crystals) (Moscow: Fizmatlit, 2008).
6. Knill E., Laflamme R., Milburn G. *Nature*, **409**, 46 (2001).
7. Kok P., Munro W.J., Nemoto K., Ralph T.C., Dowling J.P., Milburn G.J. *Rev. Mod. Phys*., **79**, 135 (2007).
8. Briegel H.-J., Dur W., Cirac J.I., Zoller P. *Phys. Rev. Lett*., **81**, 5932 (1998).
9. Tittel W., Afzelius M., Chaneliére T., Cone R.L., Kröll S., Moiseev S.A., Sellars M. *Laser Photonics Rev*., **4**, 244 (2009).
10. Simon C., Afzelius M., Appel J., Boyer de la Giroday A., Dewhurst S.J., Gisin N., Hu C.Y., Jelezko F., Kröll S., Müller J.H., Nunn J., Polzik E.S., Rarity J.G., De Riedmatten H., Rosenfeld W., Shields A.J., Sköld N., Stevenson R.M., Thew R., Walmsley I.A., Weber M.C., Weinfurter H., Wrachtrup J., Young R.J. *Eur. Phys. J. D*, **58**, 1 (2010).
11. Bussières F., Sangouard N., Afzelius M., de Riedmatten H., Simon C., Tittel W. *J. Mod. Opt*., **60**, 1519 (2013).
12. Heshami K., England D.G., Humphreys P.C., Bustard P.J., Acosta V.M., Nunn J., Sussman B.J. *J. Mod. Opt*., **63**, 2005 (2016).
13. Moiseev S.A. *Phys. Rev. A*, **83**, 12307 (2011).
14. Moiseev S.A. *Phys. Rev. A*, **88**, 12304 (2013).
15. Zhang X., Kalachev A., Kocharovskaya O. *Phys. Rev. A*, **90**, 052322 (2014).
16. Macfarlane R.M., Cassanho A., Meltzer R.S. *Phys. Rev. Lett*., **69**, 542 (1992).
17. Popova M.N., Chukalina E.P., Malkin B.Z., Saikin S.K. *Phys. Rev. B*, **61**, 7421 (2000).
18. Popova M.N. *Opt. Spectrosc*., **119**, 544 (2015).
19. Agladze N., Popova M., Zhizhin G., Egorov V., Petrova M. *Phys. Rev. Lett*., **66**, 477 (1991).
20. Macfarlane R.M., Meltzer R.S., Malkin B.Z. *Phys. Rev. B*, **58**, 5692 (1998).
21. Thiel C.W., Böttger T., Cone R.L. *J. Lumin*., **131**, 353 (2011).
22. Marino R., Lorgeré I., Guillot-Noël O., Vezin H., Toncelli A., Tonelli M., Le Gouët J.-L., Goldner P. *J. Lumin*., **169**, 478 (2016).
23. Kukharchyk N., Sholokhov D., Korableva S.L., Kalachev A.A., Bushev P.A. arXiv:1703.07621v1 [physics.optics] (2017).
24. Gerasimov K.I., Minnegaliev M.M., Malkin B.Z., Baibekov E.I., Moiseev S.A. *Phys. Rev. B*, **94**, 054429 (2016).
25. Smirnov M., Minnegaliev M., Urmancheev R., Gerasimov K., Moiseev S. *Int. Sci. Tech. Conf. 'Applied Electrodynamics, Photonics and Living Systems-2017'* (Kazan, Russia, 12–14 April) p. 539.
26. Mims W.B. *Phys. Rev*., **168**, 370 (1968).
27. Ganem J., Wang Y.P., Boye D., Meltzer R.S., Yen W.M., Macfarlane R.M. *Phys. Rev. Lett*., **66**, 695 (1991).
28. Macfarlane R.M., Wannemacher R., Boye D., Wang Y.P., Meltzer R.S. *J. Lumin*., **48**, 313 (1991).
29. Aminov L.K., Kurkin I.N., Malkin B.Z. *Fiz. Tverd. Tela*, **55**, 1249 (2013).
30. Chen Y.C., Chiang K., Hartmann S.R. *Phys. Rev. B*, **21**, 40 (1980).